Effects of Co doping in bilayered manganite $LaSr_2Mn_2O_7$: Resistivity, thermoelectric power, and thermal conductivity

R. Ang, W. J. Lu, R. L. Zhang, B. C. Zhao, X. B. Zhu, W. H. Song, and Y. P. Sun*
Key Laboratory of Materials Physics, Institute of Solid State Physics, Chinese Academy of Sciences, Hefei 230031, People's Republic of China

(Received 1 July 2005; revised manuscript received 6 September 2005; published 15 November 2005)

Systematic studies of resistivity, thermoelectric power, and thermal conductivity have been performed on polycrystalline bilayered manganites $LaSr_2Mn_{2-x}Co_xO_7$ ($0 \leqslant x \leqslant 0.2$). As $x \leqslant 0.04$, it is found that the temperature dependence of both Seebeck coefficient $S(T)$ and resistivity $\rho(T)$ in the high-temperature region follows the small polaron transport mechanism. However, in the low-temperature region, variable-range-hopping model matches the experimental data better. As $x \geqslant 0.08$, the very large magnitude of Seebeck coefficient with over 100 μV/K at low temperatures is observed, which is suggested to originate from the spin state transition of Co^{3+} ions from the intermediate-spin (IS) state or high-spin (HS) state to low-spin (LS) state and the unbalance of the spin and orbital degrees of freedom between Co^{3+} and Co^{4+} sites. In addition, the variable sign in the $S(T)$ data is observed at low temperatures for the samples with Co-doping level ($x \geqslant 0.04$), which is suggested to be related to the narrowing of accompanying band. As to thermal conduction $k(T)$, the low-temperature peak is suppressed due to Co doping. The variation of thermal conduction is analyzed based on the combined effect due to the suppression of local $Mn^{3+}O_6$ Jahn-Teller (JT) lattice distortion because of the substitution of non-JT Co^{3+} ions with LS and HS states for JT Mn^{3+} ions, which results in the increase of thermal conduction, and the introduction of the disorder due to Co doping, which contributes to the decrease of thermal conduction.

DOI: 10.1103/PhysRevB.72.184417 PACS number(s): 75.47.Lx, 74.25.Fy, 75.50.Ee

I. INTRODUCTION

The doped manganites $Ln_{1-x}A_xMnO_3$ (Ln=La, Pr, Nd, etc., and A=Ca, Sr, Ba, Pb, etc.) with perovskite structure have received considerable attention in recent years due to the discovery of colossal magnetoresistance (CMR) and more generally because of the unusually strong coupling among their charge, spin, orbit, and lattice degrees of freedom.[1–3] In this system, the mixed valence Mn^{3+}/Mn^{4+} is very important for understanding the CMR effect. In the particular context of the manganites the mixed valency leads to strong ferromagnetic (FM) interactions arising from the Mn^{3+}-O-Mn^{4+} bonds due to double-exchange (DE) mechanism.[4] In addition to DE interactions the lattice distortion is also believed to play an important role through strong electron-phonon coupling which arises from the Jahn-Teller (JT) distortion[5,6] around the Mn^{3+} ions. Furthermore, Dagotto *et al.* proposed a phase separation model where the FM metallic (FMM) and antiferromagnetic insulating (AFI) clusters coexist and their model strongly supports recent experimental studies on the physical properties of manganites.[7]

In bilayer manganites $La_{2-2x}Sr_{1+2x}Mn_2O_7$, in which a MnO_2 bilayer is alternatively stacked with a $(La,Sr)_2O_2$ blocking layer along the c axis, the physical properties strongly depend on the hole doping level.[8] In particular, neutron diffraction study has revealed the coexistence of a majority phase of the A-type AFM phase and a minority phase of CE-type AFM charge-ordered–orbital-ordered (CO-OO) phase on half doped $LaSr_2Mn_2O_7$ (x=0.5) which is of a $Sr_3Ti_2O_7$-type tetragonal cell with space group of $I4/mmm$.[9] Single crystals of bilayered manganites $La_{2-2x}Sr_{1+2x}Mn_2O_7$ with x=0.3 and 0.4 was found to exhibit an anisotropic magnetoresistance (MR) effect.[10] The anisotropy is closely associated with its layered structure having nonmagnetic insulating (La,Sr)O layers separating FMM MnO_2 bilayers. The transport properties within ab plane of a single crystal of $La_{1.2}Sr_{1.8}Mn_2O_7$ are found to resemble those of pseudocubic CMR manganites, and are interpreted using the model of two-manganese Zener polarons.[11] Moritomo *et al.*[12] have reported that the layered compound $La_{1.2}Sr_{1.8}Mn_2O_7$ is a FMM below $T_C \sim 120$ K and a paramagnetic insulator (PMI) above this temperature. They attribute the coupled electronic and magnetic transitions at T_C to the DE coupling in Mn-O-Mn linkages.

The study of the effects of Mn site doping with other elements is expected to provide important clues to the mechanism of CMR behavior because of the core role of Mn ions in CMR materials. As is well known, Co ions in perovskite cobaltites can exist in three kinds of spin states, i.e., low spin (LS), intermediate spin (IS), and high spin (HS), due to the fact that the crystal field splitting (10 Dq) of the Co d states (E_{CF}) and Hund's rule coupling energy (E_{ex}) are comparable for the cobaltites. The fact that E_{CF} and E_{ex} are comparable implies that the thermal energy ($k_BT \sim 10$ meV) can induce the spin-state transition of Co ions by thermal excitation of the t_{2g} electrons into e_g states.[13] Therefore, Co doping at Mn sites in manganites has attracted one's attention because of three kinds of spin states of Co ions and the spin-state transition.[14,15] However, very few reports have appeared on the effect of Co doping at Mn sites for bilayered perovskite manganites. Very recently, the effect of Co doping on CO state of the bilayered manganite $LaSr_2Mn_2O_7$ is investigated through the measurement of electrical and magnetic transport properties.[16] However, during the process of

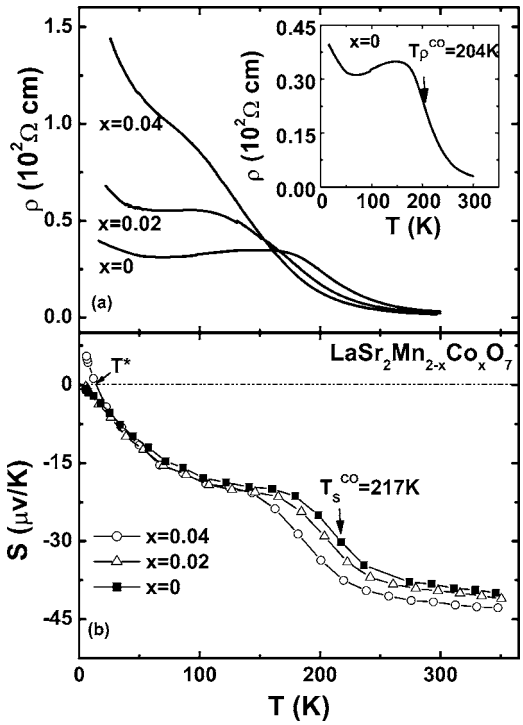

FIG. 1. (a) The temperature dependence of resistivity $\rho(T)$ and (b) the temperature dependence of Seebeck coefficient $S(T)$ for $LaSr_2Mn_{2-x}Co_xO_7$ with $x=0$, 0.02, and 0.04. Inset: the magnification plot of $\rho(T)$ curve for the $x=0$ sample.

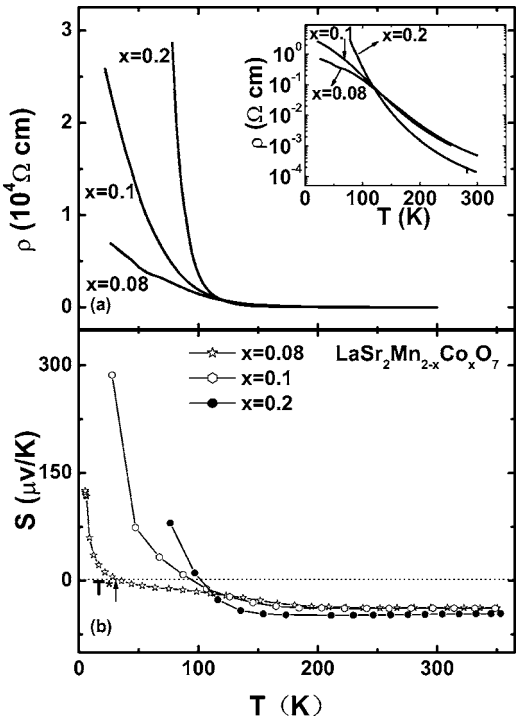

FIG. 2. (a) The temperature dependence of $\rho(T)$ and (b) the temperature dependence of $S(T)$ for $LaSr_2Mn_{2-x}Co_xO_7$ with $x=0.08$, 0.1, and 0.2 Inset: $\rho(T)$ curves in logarithm coordinates.

analyzing the transport mechanism by fitting the experimental data of resistivity ρ in the high-temperature region, we find that the temperature dependence of the resistivity $\rho(T)$ can be almost well fitted according to Mott's variable range hopping (VRH) model and adiabatic small polaronic model. That is to say, it is difficult to determine the real transport mechanism of the carriers only based on the resistivity measurement although we attributed the transport mechanism in the high temperature region to VRH transport in Ref. 16.

As we know, among various aspects of transport studies in transitional metal oxides (TMO), both thermoelectric power (TEP) S and thermal conductivity k measurements have been being important tools to investigate the transport properties of TMO as they are sensitive to the magnetic and electrical nature of charge carriers and they can present some information which can not be supplied by magnetization and resistivity measurements. In addition, S measurement is less affected by the presence of grain boundaries, which often complicates the resistivity measurement for polycrystalline samples. At the same time, S is very sensitive to the type of the charge carriers. Therefore, S and k measurement are considered to be a complementary tool to the resistivity measurement for transport property studies. Furthermore, by measuring S and k of the material, the thermoelectric figure of merit of the material can be obtained by the formula: $ZT=S^2T/\rho k$, where k is the thermal conductivity, ρ is the resistivity, S is Seebeck coefficient, and T is the absolute temperature.

In order to ravel the transport mechanism and understand fully the origin of the effect of Co doping at Mn sites in bilayered manganites, in this paper, the effect of Co doping at Mn site on ρ, S, and k of $LaSr_2Mn_{2-x}Co_xO_7$ ($0 \leqslant x \leqslant 0.2$) has been systematically studied.

II. EXPERIMENTAL

A series of bulk samples of $LaSr_2Mn_{2-x}Co_xO_7$ ($x=0$, 0.02, 0.04, 0.08, 0.1, 0.2) were synthesized by a conventional solid-state reaction method in air. Details of the sample preparation and their characterization by x-ray diffraction, magnetization measurements have been reported in Ref. 16.

The resistivity as a function of temperature was measured by a standard four-probe method from 20 to 300 K at zero field. The temperature dependence of S and k were measured by the standard four-probe method from 5 to 350 K at zero field in a commercial Quantum Design Physical Property Measurement System (PPMS) ($1.8\ \mathrm{K} \leqslant T \leqslant 400\ \mathrm{K}, 0 \leqslant H \leqslant 9\mathrm{T}$). The typical dimension of the measured sample is $4 \times 2.5 \times 1.2\ \mathrm{mm}^3$.

III. RESULTS AND DISCUSSION

A. Resistivity and TEP

The temperature dependence of resistivity $\rho(T)$ and Seebeck coefficient $S(T)$ of $LaSr_2Mn_{2-x}Co_xO_7$ samples ($0 \leqslant x \leqslant 0.2$) at zero field is shown in Figs. 1 and 2(a) and Figs. 1 and 2(b), respectively. For $x=0$ sample, inset of Fig. 1(a) shows that $\rho(T)$ curve begins to rise steeply at CO state temperature T_ρ^{CO}(=204 K) [defined from the minimum of $(d\rho/dT) \sim T$ curve]. The appearance of thermal hysteresis of

TABLE I. Parameters of the studied samples in this work. x stands for the Co-doping level. T_S^{CO} is the CO state temperature defined from $S(T)$ curves. T_N denotes the AFM transition temperature derived from the magnetization. T_ρ^{CO} is the CO state temperature defined from $\rho(T)$ curves. T_S and T_ρ express the peak temperature for $S(T)$ and $\rho(T)$ curves, respectively.

Temperature (K)	$x=0$	$x=0.02$	$x=0.04$
T_S^{CO}	217	204	182
T_N	227	207	197
T_ρ^{CO}	204	176	134
T_S	160	146	125
T_ρ	151	97	

$\rho(T)$ curve in the vicinity of T_ρ^{CO} also verifies the occurrence of CO state at T_ρ^{CO}. With decreasing temperatures further, $\rho(T)$ curve has a peak at $T_\rho=151$ K, implying there occurs a metal to insulator transition (MIT). The effect of Co doping on the resistivity of the sample has been described in detail in Ref. 16. In brief, Co doping makes both T_ρ^{CO} and T_ρ decrease and ρ increase, which is listed in Table I. As $x\geqslant 0.08$, MIT disappears and $\rho(T)$ behaves as semiconductorlike transport behavior in the whole measured temperature range.

As to $S(T)$, for Co-free sample, Fig. 1(b) shows that absolute $S(T)$ curve begins to decrease steeply in the vicinity of CO state temperature T_S^{CO}(=217 K) [defined from the minimum of $(dS/dT)\sim T$ curve]. With increasing Co-doping level, T_S^{CO} shifts to low temperatures and absolute $S(T)$ in the vicinity of T_S^{CO} slightly increases, which is suggested to be related to the destruction of A-type AFM order of $LaSr_2Mn_2O_7$ due to Co doping because $S(T)$ includes spin entropy carried by charge carriers based on the viewpoint of thermodynamics. This kind of destruction of A-type AFM order is also verified by the decrease of Néel temperature T_N.[16] In other words, the Co doping destroys partially the ordering arrangement of Mn^{3+} and Mn^{4+} leading to the gradual enhancement of spin entropy near the temperature T_S^{CO}. The more disordering arrangement between Mn^{3+} and Mn^{4+} ions because of Co doping gives rise to the decrease of T_S^{CO}. For a nearly doping-independent $S(T)$ in the low-temperature region below T_ρ as shown in Fig. 1(b), it is suggested to originate from the carrier localization effect due to the suppression of carrier hopping between MnO_2 single layers because an orbital fluctuation of $d_{x^2-y^2}$ is gradually suppressed at low temperatures and the motion of carriers are confined within respective MnO_2 single layer.[17]

In addition, for $x=0.04$ sample, Fig. 1(b) exhibits that S has a sign change and becomes positive as $T^*<10$ K. With increasing Co-doping level further, the temperature T^* at which S occurs a sign change increases as shown in Fig. 3. For the sample with $x=0.08$, 0.1, 0.2, T^* is 35, 90, 100 K, respectively, implying that the temperature range corresponding to $S>0$ becomes broader with increasing Co-doping level. The variable sign in the $S(T)$ data indicates the coexistence of two different type of carriers. As discussed in Ref. 18, a negative S at higher temperature is attributed to the

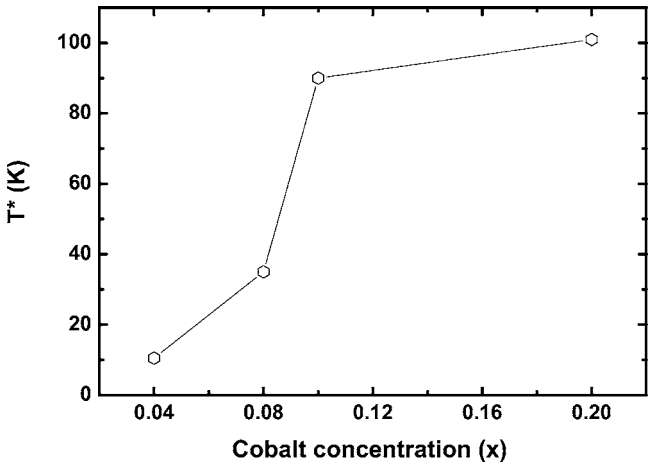

FIG. 3. The temperature T^* of $S>0$ as a function of Co-doping level for $x=0.04$, 0.08, 0.1, 0.2. The solid line is guide to the eyes.

electrons which are excited from the valence band (VB) into the conduction band (CB). Because of the higher mobility of electrons within the CB, S is negative. Nevertheless, at lower temperature, the electrons in the VB band are excited into the impurity band which generates holelike carriers, which is suggested to be responsible for a positive S. It should be expected that the negative electronlike contribution to S should become smaller when the effective band gap becomes larger. The increase of T^* with increasing Co-doping level is suggested to arise from the gradual increase of the effective band gap due to the narrowing of the concomitant $\sigma(e_g^\uparrow - 2p)$ bandwidth, where σ reflects the hybridization between Mn spin-up $e_g^\uparrow$ and O $2p$ orbitals.[18]

An interesting phenomenon is that the magnitude of S rises rapidly below T^*. The values of $S=125$ μV/K at 5 K and $S=287$ μV/K at 28 K for $x=0.08$ and 0.1 are obtained, respectively. In fact, due to the limit of measuring range, S value only can be measured at $T\geqslant 28$ K and $T\geqslant 76$ K for the samples with $x=0.1$ and 0.2. That is to say, for samples with high Co-doping level, S value at low temperatures should be expected to be much larger. On one hand, it is related to the spin state transition of Co^{3+} ion from IS (HS) state to LS state. That is to say, the remarkable enhancement of positive S may be due to the higher Seebeck coefficient of LS $Co^{3+}(t_{2g}^6 e_g^0: s=0)$ than that of $Mn^{3+}(t_{2g}^3 e_g^1: s=2)$ because Co ions lies in low spin state at low temperatures. The LS state of Co^{3+} ion is stable which is also confirmed by the appearance of the double peaks in the magnetization measurements.[16] On the other hand, the appearance of the large S is suggested to be related to the degeneracies in Co^{3+} and Co^{4+} sites and the ratio between them as in the recent theoretical calculation for the cobaltites $NaCo_2O_4$ with layered structure.[19] Directly speaking, the ground state of Co^{3+} (nonmagnetic) ion is considered to lie in the LS state with $S=0$ and Co^{4+} (magnetic ion) sites may be in the HS and LS states for present studied system. The numbers of configurations (denoting the degeneracy) in Co^{3+} and Co^{4+} sites are determined by the crystal-field splitting energy E_{CF}, the Hund's rule coupling energy E_{ex}, and the thermal energy k_BT. Generally speaking, if one does not consider crystal field, both Co^{3+} and Co^{4+} ions are in the HS states due to the large

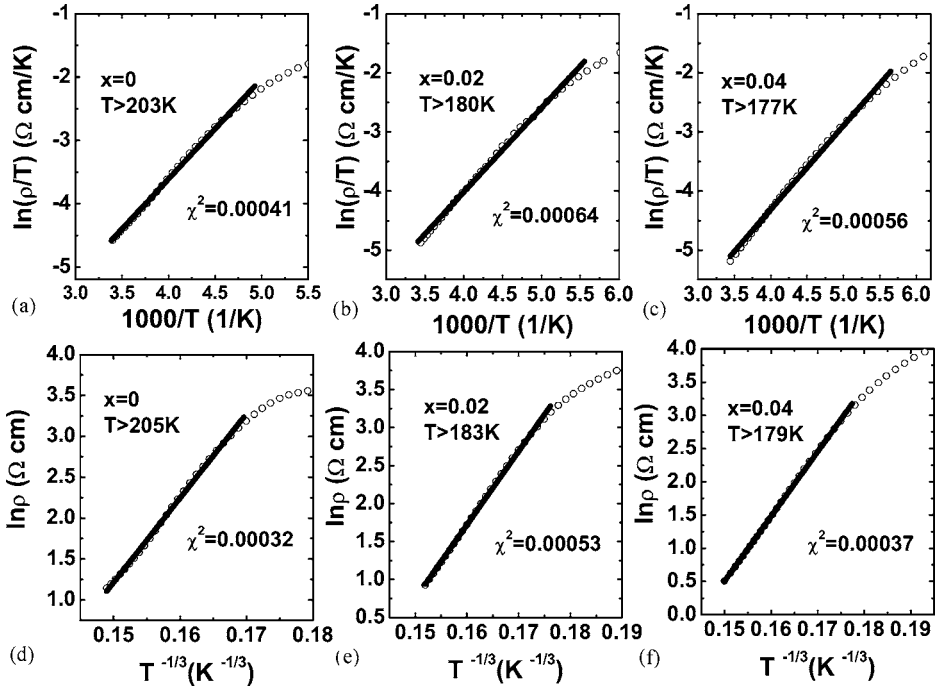

FIG. 4. (a)–(c) the plot of $\ln(\rho/T)$ vs $1000/T$ for $LaSr_2Mn_{2-x}Co_xO_7$ ($x=0$, 0.02, and 0.04) in the high-temperature region and (d)–(f) the plot of $\ln\rho$ against $T^{-1/3}$ in the high-temperature region. The solid lines of (a)–(c) and (d)–(f) correspond to the fitting by SPC model and Mott's VRH model, respectively. The parameter χ^2 (reduced chi-square value of fit) represents the quality of the fit.

coupling energy E_{ex} ($k_BT \ll E_{ex}, E_{CF} \ll E_{ex}$) with $S=2$ and $S=5/2$, respectively. However, with taking into account the octahedral crystal field, the energies of LS and IS states reduce relative to that of HS state. As E_{CF} reaches a special value, the LS state of Co^{3+} site becomes stable, and the HS and LS states of Co^{4+} are close in energy ($k_BT \ll E_{CF}, E_{ex}$). Consequently, the number of configuration in Co^{3+} site is much smaller than that of Co^{4+} site, which results in a large S value. In addition, for samples with high Co-doping level of $x \geqslant 0.08$, a nearly doping-independent and temperature-independent $S(T)$ in the high-temperature region is also observed as shown in Fig. 2(b). In the following, we will focus on analyzing the transport mechanism of $LaSr_2Mn_{2-x}Co_xO_7$ samples combined with ρ and S data.

1. High-temperature ($T > T_\rho$) transport mechanism for Co-free and lightly Co-doped samples $LaSr_2Mn_{2-x}Co_xO_7$ *($x=0, 0.02$, and 0.04)*

In the high-temperature region of $T > T_\rho$, resistivity $\rho(T)$ data at zero field are fitted by thermally activated conduction (TAC) law $\rho(T)=\rho_0 \exp(E_0/k_BT)$, the adiabatic small polaronic conduction (SPC) $\rho=\rho_0 T \exp(E_\rho/k_BT)$, and the two-dimensional Mott's VRH model $\rho(T)=\rho_0 \exp[(T_0/T)^{1/3}]$, with $T_0 \approx 21/[k_BN(E_F)\xi^3]$, where ξ is the localization length, $N(E_F)$ is the density of localized states at the Fermi energy, and E_0 and E_ρ is the activation energy.[20] It is found that both SPC model and VRH model match the resistivity data well in the high temperature region ($T > T_\rho$). For the sample with $x=0$, 0.02, and 0.04, the plot of $\ln(\rho/T)$ vs $1000/T$ and the plot of $\ln\rho(T)$ against $T^{-1/3}$ are shown in Figs. 4(a)–4(c) and Figs. 4(d)–4(f), respectively. To provide a clearer distinction between SPC model and VRH model, we have plotted the data in a smaller range. The scatter symbols correspond to the experimental data and the solid lines denote the fitted results according to SPC model [Figs. 4(a)–4(c)] and Mott's VRH model [Figs. 4(d)–4(f)], respectively. The values of activation energy E_ρ and characteristic temperature $T_{0\rho}^H$ [denoting the values of T_0 in the high-temperature region obtained by fitting $\rho(T)$ data] are listed in Tables II and III, respectively. In addition, the parameter χ^2 (reduced chi-square value of fit) related to the quality of the fit is also

TABLE II. Both E_ρ and E_S are activation energies calculated by fitting $\rho(T)$ and $S(T)$ curves according to SPC model for the sample with Co-doping level of $x=0$, 0.02, and 0.04 in the high-temperature region. W_H is the hopping energy of the small polaron in a given direction. E_p is the formation energy of the small polaron. The α is a fitting parameter. "±" stands for the error which forms by fitting $\rho(T)$ and $S(T)$ data.

Parameter	$x=0$	$x=0.02$	$x=0.04$
E_ρ (meV)	125.93±0.69	131.96±0.86	139.73±0.78
E_S (meV)	5.65±0.02	5.39±0.02	4.68±0.03
W_H/k_B (K)	1395	1467	1566
E_p (meV)	240.56	253.14	270.10
α	−0.582±0.002	−0.577±0.002	−0.573±0.001

TABLE III. The fitting parameters of $S(T)$ and $\rho(T)$ curves according to the two-dimension VRH model (see text) in the high- and low-temperature regions. T_{0S}^H and $T_{0\rho}^H$ stand for the characteristic temperature in the high-temperature region for $S(T)$ and $\rho(T)$, respectively. A is a fitting parameter for $S(T)$ in the low-temperature region. $T_{0\rho}^L$ denotes the characteristic temperature in the low region for $\rho(T)$. "±" expresses the error which produces by fitting $\rho(T)$ and $S(T)$ data.

Co content	$(T_{0S}^H)^{1/3}$	$(T_{0\rho}^H)^{1/3}$	A (μV K$^{-3/2}$)	$(T_{0\rho}^L)^{1/3}$
$x=0$	540.17±0.37	96.80±0.03	4.89±0.02	1.58±0.01
$x=0.02$	536.78±0.54	96.95±0.11	5.04±0.04	2.25±0.01
$x=0.04$	504.48±0.46	97.38±0.08	6.11±0.07	3.62±0.01

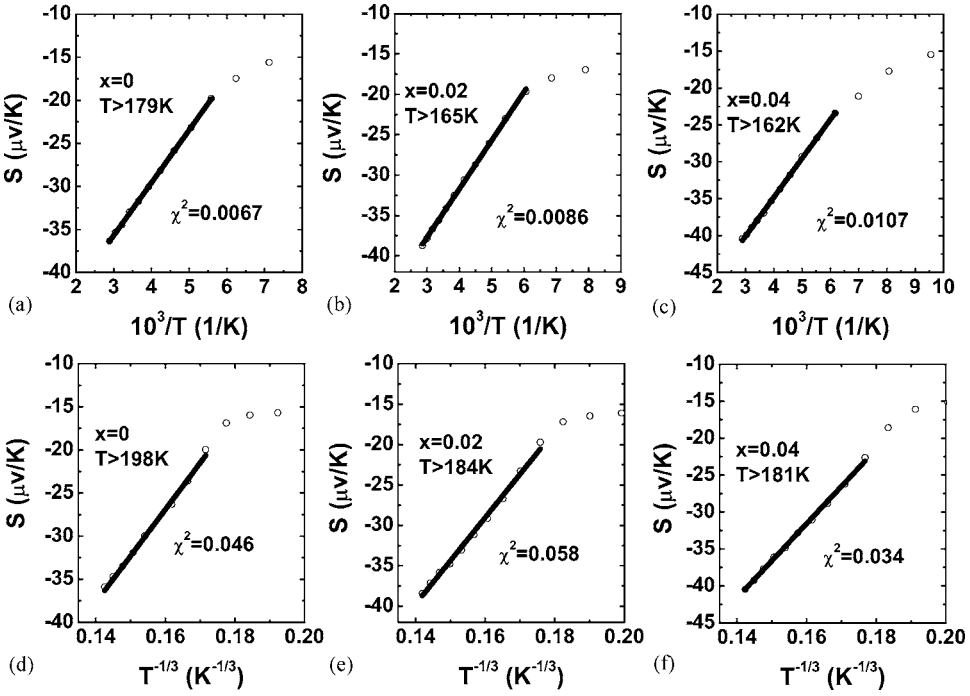

FIG. 5. (a)–(c) The plot of S vs $1000/T$ for $LaSr_2Mn_{2-x}Co_xO_7$ ($x=0$, 0.02, and 0.04) in the high-temperature region and (d)–(f): the plot of S vs $T^{-1/3}$ in the high-temperature region. The solid lines of (a)–(c) and (d)–(f) correspond to the fitting by SPC model and VRH model, respectively. The parameter χ^2 denotes the quality of the fit.

shown in Fig. 4. Unfortunately, only based on the fitting results of $\rho(T)$ data, it is difficult to determine the real transport mechanism of the carriers because of the nearly same fitting temperature region and the close quality of the fit for SPC and VRH models. Hence, it is necessary to perform the fitting of $S(T)$.

As is well known, if the polaronic conduction dominates the carrier transport, $S(T)$ should be described by the following equation:[20]

$$S(T) = k_B/e[E_S/k_BT + \alpha], \tag{1}$$

where k_B is Boltzmann's constant, e is the electron's charge, E_S is the activation energy obtained according to the fitting of the $S(T)$ data, and α is a sample-dependent constant, which is associated with the spin and the mixing entropy.[21] In addition, $\alpha<1$ suggests the conduction is the small polaron hopping and $\alpha>2$ represents the existence of a large polaron.[22] For SPC, another character is $E_S \ll E_\rho$, E_ρ is a fitted activated energy according to SPC formula based on $\rho(T)$ curves.

Comparatively, if Mott's VRH dominates the carrier transport, $S(T)$ in the high-temperature region ($T>T_\rho$) should meet following relationship:[23]

$$S(T) \propto \left(\frac{T_{0S}}{T}\right)^{1/3} \tag{2}$$

where T_{0S} is the characteristic temperature similar to the temperature T_0 of the VRH formula of $\rho(T)$ mentioned above.

In order to test above two models, the curves of S vs $1000/T$ and S against $T^{-1/3}$ for the samples $x=0$, 0.02, and 0.04 are plotted in Figs. 5(a)–5(f), respectively. The scatter symbols correspond to the experimental data and the solid lines denote the fitted results according to Eq. (1) [Figs. 5(a)–5(c)] and Eq. (2) [Figs. 5(d)–5(f)], respectively. The fitting parameters values of E_S, α, and T_{0S}^H [denoting the values of T_{0S} in the high-temperature region obtained by fitting $S(T)$ data] are listed in Tables II and III, respectively. To distinguish SPC model from VRH model well, the parameter χ^2 of the fitting quality is indicated in Fig. 5. First, the fitting result of $\alpha<1$ implies that SPC dominates the transport of the carriers for low Co-doping level of $x \leqslant 0.04$ in the high-temperature region of $T>T_\rho$.[22] Secondly, based on Fig. 5, it exhibits that the fitting temperature range of Eq. (1) as shown in Figs. 5(a)–5(c) is more wider (>20 K) than that of Eq. (2) as shown in Figs. 5(d)–5(f). Thirdly, the value of χ^2 in the SPC model is nearly one order of magnitude smaller than that in the VRH model, implying that the accuracy of the fit for SPC model is better than that for VRH model. Accordingly, the SPC model is really superior to VRH model in describing the transport of the carriers in the high-temperature region of $T>T_\rho$ from the viewpoint of the fitting results of S data. In addition, from Table II, it is clearly seen that E_S gradually decreases and E_ρ increases with increasing Co-doping level. Moreover, the magnitude of E_S is much smaller than that of E_ρ, which is the character of SPC mentioned above. In brief, in the framework of the SPC model, E_ρ is the sum of the activation energy needed for the creation of the carriers and activating the hopping of carriers, and E_S is the energy required to activate the hopping of carriers. Hence, E_S is much smaller than E_ρ. Additionally, based on E_ρ and E_S, both the polaronic hopping energy $W_H=E_\rho-E_S$ and the polaronic formation energy $E_p=2W_H$ can be obtained as denoted in Table II. As to the variation of E_S and E_ρ with the Co-doping level, they can be attributed to the decreasing of the width for the polaron band gap and to the increasing of the localization of the carriers, respectively.[24]

In a word, based on the fitting temperature range and fitting parameters of $S(T)$ described above, the conclusion

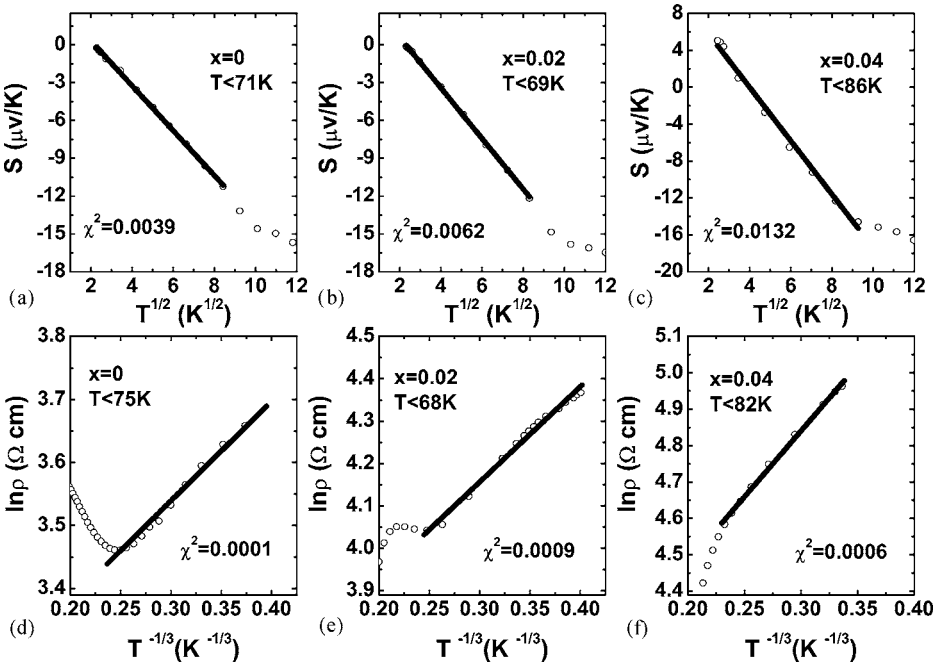

FIG. 6. (a)–(c) The plot of $\ln \rho$ against $T^{-1/3}$ for $LaSr_2Mn_{2-x}Co_xO_7$ ($x=0$, 0.02, and 0.04) in the low-temperature region and (d)–(f) the plot of S vs $T^{1/2}$ in the low-temperature region. The solid lines are the fitting data according to the VRH model. The parameter χ^2 stands for the quality of the fit.

that the transport mechanism is mainly dominated by SPC in the high-temperature region of $T>T_\rho$ for the sample with low Co-doping level of $x\leqslant 0.04$ can be drawn. Additionally, in the bilayered manganites, the character of the small polaron is also reflected in the fact that the magnitudes of both T_N and T_S are larger than that of T_ρ as shown in Table I.[25]

2. *Low-temperature* ($T<T_\rho$) *transport mechanism for* $LaSr_2Mn_{2-x}Co_xO_7$ ($x=0, 0.02$, and 0.04)

In order to analyze the transport mechanism of the samples with Co-doping level of $x\leqslant 0.04$ in the low-temperature region of $T<T_\rho$, both ρ and S data are fitted according to SPC model described above (not shown here) and VRH model. The curves of $\ln \rho(T)$ against $T^{-1/3}$ and S vs $T^{1/2}$ for the samples $x=0$, 0.02, and 0.04 are plotted in Figs. 6(a)–6(c) and Figs. 6(d)–6(f), respectively, indicating that ρ data can be described by the two dimensional Mott's VRH formula mentioned above and S data meets the following relationship:[26,27]

$$|S| = A(T)^{1/2} + B \tag{3}$$

with $A=(k_B/3e)\zeta^2 T_0^{1/2}[d \ln N(\varepsilon)/d\varepsilon]_{\varepsilon=0}$, where ζ is a factor which determines the thickness of the energy layer within which the states are effective in conduction, $N(\varepsilon)$ is density of state (DOS), ε is the energy measured from the Fermi level, and B is a constant which is the intrasite correlation contribution. The in-depth derivation for these parameters of Eq. (3) can be found in the literature.[28] The fitting parameters $T_{0\rho}^{L}$ [denoting the values of T_0 in the low-temperature region obtained by fitting $\rho(T)$ data] and A are listed Table III. The parameter χ^2 of the fitting quality is also plotted in Fig. 6. The Table III shows that $T_{0\rho}^{L}$ enhances with increasing Co-doping level, implying the localization of the carrier increases with increasing Co-doping level if the variation of $N(\varepsilon)$ in the vicinity of Fermi surface is not considered. In addition, the fact that A changes little with increasing Co-doping level is suggested to originate from the carrier localization effect as discussed above. Therefore, the transport mechanism in the low temperature region ($T<T_\rho$) for the samples of $x=0$, 0.02, and 0.04 can be suggested to originate from VRH of the carriers.

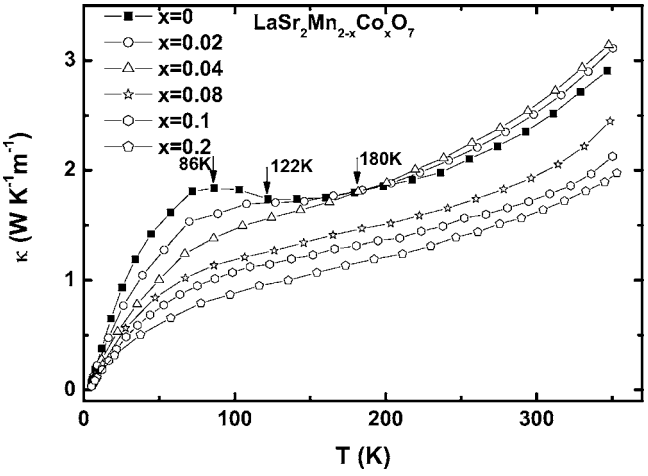

FIG. 7. The temperature dependence of the measured total k of $LaSr_2Mn_{2-x}Co_xO_7$ ($x=0$, 0.02, 0.04, 0.08, 0.1, 0.2).

3. *Transport mechanism for heavily Co-doped samples* $LaSr_2Mn_{2-x}Co_xO_7$ ($x=0.08, 0.1$, and 0.2)

For the samples of $x\geqslant 0.08$, it is found that neither SPC model nor VRH model matches the S data in the high- and low-temperature regions. However, Mott's VRH model matches ρ data well in high- and low-temperature region as described in Ref. 16. Especially for $x=0.2$ sample, the ρ data

TABLE IV. The values of the measured total k and k_{ch} calculated from WF law for the sample $LaSr_2Mn_{2-x}Co_xO_7$ ($0 \leqslant x \leqslant 0.2$) at 100 K.

Co content	$x=0$	$x=0.02$	$x=0.04$	$x=0.08$	$x=0.1$	$x=0.2$
k (W K^{-1} m^{-1})	1.82	1.69	1.49	1.21	1.07	0.86
k_{ch} (W K^{-1} m^{-1})	7.6×10^{-6}	4.2×10^{-6}	2.9×10^{-6}	1.6×10^{-7}	1.2×10^{-7}	7.2×10^{-9}

can be fitted within whole measured temperature region, implying the localization of the carriers enhances dramatically. We know that the remarkable localization of charge carriers for the samples with heavy Co-doping level gives rise to a nearly invariable spin entropy, which results in a nearly doping-independent and temperature-independent $S(T)$ in the high-temperature region.

As to the large positive S value for the samples with high Co-doping level, we consider that it may be related to the spin state transition of Co^{3+} ions from IS (HS) state to LS state and the unbalance of the spin and orbital degrees of freedom between Co^{3+} and Co^{4+} sites as mentioned above.

In short, VRH may dominate the transport of the carriers in the high- and low-temperature region for the sample with high Co-doping level of $x \geqslant 0.08$ although S data cannot be fitted according to VRH model.

B. Thermal conductivity

The temperature dependence of thermal conductivity $k(T)$ of $LaSr_2Mn_{2-x}Co_xO_7$ samples ($0 \leqslant x \leqslant 0.2$) at zero field is shown in Fig. 7. Usually, the k can be expressed by the sum of phononic component (k_{ph}) and mobile charge carriers component (k_{ch}) as $k=k_{ph}+k_{ch}$. The k_{ch} value can be estimated from Wiedemann-Franz (WF) law, which relates k_{ch} to ρ according to $k_{ch}=L_0T/\rho$, where $L_0=2.44\times10^{-8}$ V^2/K^2 denotes the Lorenz number. Consequently, k_{ph} can be obtained by subtracting k_{ch} from k. The values of k and k_{ch} calculated according to WF law at 100 K are listed in Table IV, indicating that the k_{ch} value is much lower than that the k value. So the measured k is suggested to come from the contribution of the k_{ph} due to the negligible contribution of the k_{ch}.

For Co-free sample, $k(T)$ seems to be consistent with usual phononic heat transport. However, a closer observation of the $k(T)$ reveals an anomalous feature. The k decreases with increasing temperatures in 86 K $< T <$ 122 K, implying that an unusual additional scattering mechanism may be active above 86 K. For Co-doping samples with $x=0.02$ and 0.04, the $k(T)$ behavior is similar to that of Co-free sample. However, the low-temperature k peak is strongly suppressed with increasing Co-doping level. Interestingly, the k increases with increasing Co-doping level in the high-temperature region of $T>180$ K for $x=0.02$, 0.04, which is different from the k behavior in the low-temperature region of $T<180$ K.

As we know, for Co-free sample, the local $Mn^{3+}O_6$ Jahn-Teller (JT) lattice distortion due to Mn^{3+} JT ions can scatter the phonon, which gives rise to the decrease of k. As Mn^{3+} ions are partially substituted by non-JT Co^{3+} ions with LS and HS states, the local $Mn^{3+}O_6$ JT lattice distortion is suppressed, which results in the increase of k.[29] Although the disorder introduced due to Co doping scatters the phonon, which contributes the reduction of k, it is suggested that the former k contribution dominates in the high-temperature region of $T>180$ K for low Co-doping samples of $x=0.02$ and 0.04. As to the drastic suppression of k at low temperatures for low Co-doping samples, it is suggested to arise from the disorder due to the Co doping, which hinders a strong increase of the mean free path of the phonon for $T \to 0$ K.

For the sample with high Co-doping level of $x \geqslant 0.08$, Fig. 7 shows that the k is reduced over a whole range of temperature. The decrease of the k is suggested to originate from the combined effect due to the introduction of the disorder because of Co doping, which results in the decrease of thermal conduction, exceeds the effect of the suppression of local $Mn^{3+}O_6$ JT lattice distortion due to the substitution of non-JT Co^{3+} ions with LS and HS states for JT Mn^{3+} ions, which leads to the increase of thermal conduction.

IV. CONCLUSION

In summary, the effects of Co-doping on ρ, S, and k in bilayered manganite $LaSr_2Mn_{2-x}Co_xO_7$ ($0 \leqslant x \leqslant 0.2$) have been investigated systematically. For low Co-doping samples of $x \leqslant 0.04$, the SPC mechanism is verified by fitting $S(T)$ and $\rho(T)$ curves in the high-temperature region. However, in the low-temperature region, VRH mechanism dominates the transport of the sample. As $x \geqslant 0.08$, the very large magnitude of S with over 100 μV/K at low temperatures is observed, which is suggested to originate from the spin state transition of Co^{3+} ions from IS (HS) state to LS state, the degeneracies and the ratio between Co^{3+} and Co^{4+} sites. Additionally, the mechanism of variable sign in the $S(T)$ data is also analyzed according to two-band model. As to the k, the low-temperature k peak is suppressed due to Co doping. The effect of the Co doping on the k is discussed in terms of the combined effect due to the suppression of local $Mn^{3+}O_6$ JT lattice distortion because of the substitution of non-JT Co^{3+} ions with LS and HS states for JT Mn^{3+} ions, which results in the increase of thermal conduction, and the introduction of the disorder due to Co doping, which contributes to the decrease of thermal conduction.

ACKNOWLEDGMENTS

This work was supported by the National Key Basic Research under Contract No. 001CB610604, and the National Nature Science Foundation of China under Contract Nos. 10174085, 10474100, 10374033 and Fundamental Bureau of Chinese Academy of Sciences.

*Electronic address: ypsun@issp.ac.cn

[1] S. Jin, T. H. Tiefel, M. McCormack, R. A. Fastnacht. R. Ramesh, and L. H. Chen, Science **264**, 413 (1994).
[2] A. Asamitsu, Y. Moritomo, Y. Tomioka, T. Arima, and Y. Tokura, Nature (London) **373**, 407 (1995).
[3] R. von Helmolt, J. Wecker, B. Holzapfel, L. Schultz, and K. Samwer, Phys. Rev. Lett. **71**, 2331 (1993).
[4] C. Zener, Phys. Rev. **82**, 403 (1951); P. G. de Gennes, *ibid.* **118**, 141 (1960).
[5] J. B. Goodenough, Phys. Rev. **100**, 564 (1955).
[6] A. J. Millis, P. B. Littlewood, and B. J. Shraiman, Phys. Rev. Lett. **74**, 5144 (1995).
[7] E. Dagotto, T. Hotta, and A. Moreo, Phys. Rep. **344**, 1 (2001).
[8] K. Hirota, Y. Moritoma, H. Fujioka, M. Kubota, H. Yashizawa, and Y. Endoh, J. Phys. Soc. Jpn. **68**, 1463 APR (1999).
[9] M. Kubota, H. Yoshizawa, Y. Moritomo, H. Fujioka, K. Hirota, and Y. Endoh, J. Phys. Soc. Jpn. **68**, 2202 (1999).
[10] T. Kimura, A. Asamitsu, H. Kuwahara, and Y. Tokura, Phys. Rev. Lett. **79**, 3720 (1997).
[11] J.-S. Zhou, J. B. Goodenough, and J. F. Mitchell, Phys. Rev. B **58**, R579 (1998).
[12] Y. Moritomo, A. Asamitsu, H. Kuwahara, and Y. Tokura, Nature (London) **380**, 141 (1996).
[13] S. R. English, J. Wu, and C. Leighton, Phys. Rev. B **65**, 220407 (2002).
[14] N. Gayathri, A. K. Raychaudhuri, S. K. Tiwary, R. Gundakaram, Anthony Arulraj, and C. N. R. Rao, Phys. Rev. B **56**, 1345 (1997).
[15] C. M. Srivastava, Santanu Banerjee, T. K. GunduRao, A. K. Nigam, and D. Bahadur, J. Phys.: Condens. Matter **15**, 2375 (2003).
[16] R. L. Zhang, W. H. Song, Y. Q. Ma, J. Yang, B. C. Zhao, Z. G. Sheng, J. M. Dai, and Y. P. Sun, Phys. Rev. B **70**, 224418 (2004).
[17] T. Kimura, R. Kumai, Y. Tokura, J. Q. Li, and Y. Matsui, Phys. Rev. B **58**, 11 081 (1998).
[18] J. Fontcuberta, A. Seffar, X. Granados, J. L. Garcia-Munoz, X. Obradors, and S. Pinol, Appl. Phys. Lett. **68**, 16 (1996).
[19] W. Koshibae, K. Tsutsui, and S. Mackawa, Phys. Rev. B **62**, 6869 (2000).
[20] N. F. Mott and E. A. Davis, in *Electronics Process in Non Crystalline Materials* (Clarendon, Oxford, 1971).
[21] M. Jaime, M. B. Salamon, M. Rubinstein, R. E. Treece, J. S. Horwitz, and D. B. Chrisey, Phys. Rev. B **54**, 11914 (1996).
[22] K. Sega, Y. Kuroda, and H. Sakata, J. Mater. Sci. **33**, 1303 (1998).
[23] I. P. Zvyagin, Fiz. Tekh. Poluprovodn. (S.-Peterburg) **12**, 1018 (1978).
[24] S. G. Wang, K. B. Li, Z. X. Chen, and Y. H. Zhang, Phys. Rev. B **61**, 575 (2000).
[25] N. H. Hur, Jin-Tae Kim, K. H. Yoo, Y. K. Park, and J.-C. Park, Phys. Rev. B **57**, 10 740 (1998).
[26] I. P. Zvyagin, Phys. Status Solidi B **58**, 443 (1973).
[27] H. Overhof, Phys. Status Solidi B **67**, 709 (1975).
[28] I. P. Zvyagin, in *Hopping Transport in Solids*, edited by M. Pollak and B. Shklovskii (North-Holland, Amsterdam, 1991), Vol. 28, Chap. 5, pp. 143–174; M. A. Buhannic, M. Danot, P. Colombet, P. Dordor, and G. Fillion, Phys. Rev. B **34**, 4790 (1986).
[29] M. Matsukawa, M. Narita, T. Nishimura, M. Yoshizawa, M. Apostu, R. Suryanarayanan, A. Revcolevschi, K. Itoh, and N. Kobayashi, Phys. Rev. B **67**, 104433 (2003).